Proton uptake mechanism of bacteriorhodopsin as determined by time-resolved stroboscopic-FTIR-spectroscopy

Georg Souvignier and Klaus Gerwert
Max-Planck-Institut für Ernährungsphysiologie, Rheinlanddamm 201, 4600 Dortmund 1, Germany

ABSTRACT Bacteriorhodopsin's proton uptake reaction mechanism in the M to BR reaction pathway was investigated by time-resolved FTIR spectroscopy under physiological conditions (293 K, pH 6.5, 1 M KCl). The time resolution of a conventional fast-scan FTIR spectrometer was improved from 10 ms to 100 μs, using the stroboscopic FTIR technique. Simultaneously, absorbance changes at 11 wavelengths in the visible between 410 and 680 nm were recorded. Global fit analysis with sums of exponentials of both the infrared and visible absorbance changes yields four apparent rate constants, k_7 = 0.3 ms, k_4 = 2.3 ms, k_3 = 6.9 ms, k_6 = 30 ms, for the M to BR reaction pathway. Although the rise of the N and O intermediates is dominated by the same apparent rate constant (k_4), protein reactions can be attributed to either the N or the O intermediate by comparison of data sets taken at 273 and 293 K. Conceptionally, the Schiff base has to be oriented in its deprotonated state from the proton donor (asp 85) to the proton acceptor (asp 96) in the M_1 to M_2 transition. However, experimentally two different M intermediates are not resolved, and M_2 and N are merged. From the results the following conclusions are drawn: (*a*) the main structural change of the protein backbone, indicated by amide I, amide II difference bands, takes place in the M to N (conceptionally M_2) transition. This reaction is proposed to be involved in the "reset switch" of the pump, (*b*) In the M to N (conceptionally M_2) transition, most likely, asp-85's carbonyl frequency shifts from 1,762 to 1,753 cm^{-1} and persists in O. Protonation of asp-85 explains the red-shift of the absorbance maximum in O. (*c*) The catalytic proton uptake binding site asp-96 is deprotonated in the M to N transition and is reprotonated in O.

INTRODUCTION

The membrane protein bacteriorhodopsin of Halobacterium halobium acts as a light driven proton pump (for a recent review see reference 1). Several approaches have been made to investigate the photocycle. Most of them are based on absorbance change measurements in the UV visible spectral range between 300 and 700 nm (for recent articles see references 2, 3 and papers cited therein). Absorbance changes in this region are due to changes of the retinal and its microenvironment. Detailed information about the chromophore structure on the single bond level is yielded by resonance-Raman (RR) experiments (for review see references 4, 5). Measurements of infrared absorbance changes gave insight into not only the chromophore but also the protein backbone and side-group reactions (for review see reference 6). A number of absorbance bands in the RR and IR spectra are assigned to vibrations of specific molecular groups using isotopically labeled and site-specific mutated BR molecules (4–9). The time course of the charge displacement during the photocycle was monitored by electric charge measurements (for review see reference 10).

The originally proposed unidirectional photocycle of BR, without significant back reactions, cannot explain all the experimental results (11). The biphasic decay of the blue shifted M intermediate alone has to include back reactions, branching, or parallel cycles. As a consequence, there is always a larger number of intrinsic rate constants than there are apparent, i.e., measurable, constants. This leads to a multitude of model schemes which connect these intermediates with first order reactions. Two principal different proposals are given: parallel photocycles originating from different BR ground states (12–14) or a linear photocycle with significant back reactions particularly during the M- to BR-reaction pathway (3, 15).

We have measured the absorbance changes during the bacteriorhodopsin photocycle between 1,800 and 1,000 cm^{-1} with a spectral resolution of 4 cm^{-1} using the stroboscopic FTIR-technique (16, 17). We achieved a time resolution of 100 μs compared with the 10 ms in an earlier approach using the rapid scan technique (18). Importantly, in the experiments described here, the salt concentration of the sample is drastically increased (1 M KCl), compared with the other approaches (17, 18, 24). Simultaneously, absorbance changes in the visible spectral range were monitored in order to compare the IR data with other experiments (19). The absorbance data of both spectral ranges are analyzed by a Global-Fit procedure that assumes first order reactions, i.e., the data are approximated by sums of exponentials yielding apparent rate constants (18). The implications of our results for photocycle models and the proton uptake mechanism are discussed.

MATERIALS AND METHODS

Sample preparation

Purple membrane (PM) was isolated as described in reference 20. 440 μl of PM suspension with OD 0.5, 20 mM KCl and buffered to pH 6.5 with Hepes buffer were dried on two CaF_2 windows under a nitrogen stream. The two films were cooled and subsequently rehydrated. They

This paper is dedicated to Benno Hess on the occasion of his 70th birthday.

Address correspondence to Klaus Gerwert.

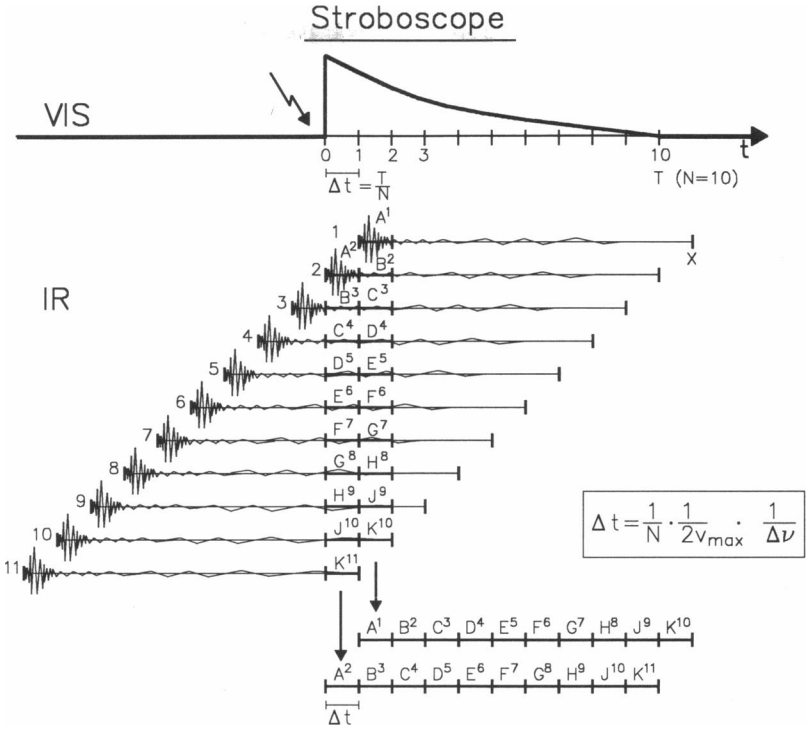

FIGURE 1 Scheme stroboscope technique. The reaction is indicated by an absorbance change in the visible (*VIS*). In 11 succeeding experiments inferograms are measured (*IR*) which are shifted relative to the VIS signal. New inferograms (*lower part*) with increased time resolution are composed from segments of the measured interferograms.

then were pressed together separated by a 2.5 μm spacer and placed in a home-made sample chamber. The ionic strength in this preparation was ~3 M. Photocycle kinetics of this sample were taken at seven wavelengths in the visible spectral region at room temperature and compared with those of a suspension. Agreement between the photocycle kinetics of the two sample preparations indicates sufficient hydration.

Measuring conditions

At 293 K absorbance changes in the IR from 1,800 to 1,000 cm^{-1} and at 11 wavelengths between 410 and 680 nm were recorded simultaneously. The absorbance change at 410 nm was measured every 30 min as a control during the 7-h measuring time.

Stroboscopic FTIR

The data acquisition for this time-resolved FTIR technique is done by the fast-scan mode (18). By merely introducing software changes, the stroboscope method allows our experimental set up to achieve a time resolution of 110 microseconds. The idea (21) is this: if it takes a time T to monitor a complete interferogram of length X, it only takes T/N time to record an X/N segment of the interferogram. Successive experiments record all N different interferogram segments and software sorts and combines these segments into the appropriate interferograms with a T/N time resolution. Fig. 1 illustrates an absorbance change in the visible (VIS) signals protein activity. We divide the interferograms of length X into ten ($N = 10$) segments. The start of the nth interferogram relative to the excitation is at a time:

$$\frac{n \cdot X}{10}, \quad n = 1, 2 \cdots$$

The newly rearranged interferogram ($A^2\ B^3 \cdots K^{11}$) has 10 times the original time resolution (see Fig. 1). Because each measured interferogram contains several useful segments (e.g., B^2 in interferogram 2, C^3 in interferogram 3) the multiplex advantage persists although to a lesser degree as N increases. The loss of the multiplex advantage makes this method more time consuming with increasing time resolution. Importantly, the Jaquinot advantage is still present, thus requiring less averages for each segment than with dispersive instruments. The stroboscopic FTIR technique requires a high degree of stability of all parts of the apparatus. Drifts in one component, e.g., the flash intensity, the detector response, or the BR sample, would lead to artifacts in the rearranged interferogram. FT transforms such interferogram inconstancies into artificial structures in the spectra which in the worst cases render them useless or cause misinterpretations. Another precondition is a constant mirror velocity during the data acquisition.

The interferograms contain a superimposed intensity change induced by the laser flash (Fig. 2, *a* and *b*). These changes seem to come from photocycle reactions, because only photoactive PM, but not dried or bleached PM, caused this signal. Furthermore, the time course of the intensity change qualitatively exhibits the same temperature dependence as the photocycle. A linear superposition of all absorbance changes in the IR can be excluded, because it cannot be described as a sum of exponentials, whereas all absorbance changes in the IR can be fitted well by such functions. This intensity change results in the superposition of the composed interferograms with a periodic function, leading to artificial bands in the difference spectra. The interferograms are corrected such that the artifacts only cover a small region in the difference spectra with spectral width of ~10 cm^{-1}. Since this distortion in the interferograms is periodic, the artifacts are also periodic. The fewer the artifacts, the further apart they lie. It is easy to calculate the position in the spectrum at which they are expected. Under our conditions, they were separated by 658 cm^{-1} resulting in only one artifact at 1,316 cm^{-1} between 1,800 and 1,000 cm^{-1}. As a control FTIR measurements were performed at 288 K on the same sample applying fast-scan and stroboscopic FTIR. They confirmed the artifact at 1,316 cm^{-1} as the only one in the stroboscopic measurement. These results prove that it is possible

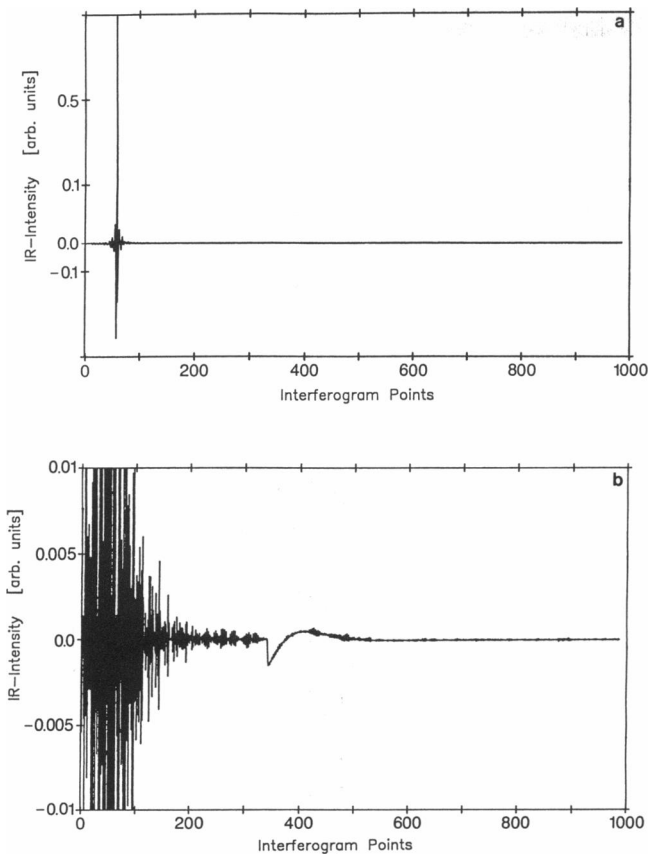

FIGURE 2 (*a*) An interferogram is shown; (*b*) an expanded scale the light induced intensity change during photocycling bacteriorhodopsin.

to exclude misinterpretations due to that kind of artifact under our measuring conditions.

Global-Fit-Evaluation

The time course of the absorbance changes in the visible and the infrared were analyzed by a global fitting (35) with sums of nr exponentials with the rate constants k_i to the data

$$\Delta A(\nu) = \sum_{i=1}^{nr} a_1(\nu) * e^{-k_i t} + a_0.$$

In this analysis, the weighted sum of squared differences between the fit with nr rate constants k_i and data points at nw measured wavelengths ν_i and nt time t_j.

$$f = \sum_{i=1}^{nw} \sum_{j=1}^{nt} [w_j(\nu_i)]^2 * [\Delta A_{\text{measured}}(\nu_i, t_j) - \sum_{i=1}^{nr} a_i(\nu_i) * e^{-k_i t_j} + a_0(\nu_i)]^2$$

is minimized in one procedure assuming the rate constants are the same for all spectral elements. The weights $w_j(\nu_i)$ are chosen with respect to the estimated noise at each wavelength (18). This is important for IR data because the amplitudes of the noise differ by more than one order of magnitude over the observed spectral range. The criteria for the significance of an additional rate constant were: (*a*) the sum of squared differences between fit and data of all wavenumbers is lowered significantly; (*b*) the sum of squared differences between fit and data of some neighboring wavenumbers is lowered significantly; (*c*) after addition of a new rate constant the residual plot of one or more wavenumbers is significantly moved towards a random distribution.

The last conditions are important because the improvement depends on the signal to noise ratio (SNR). Sometimes the overall sum of squares happens to improve only by a small amount. In this case an additional rate constant is required at some wavenumbers for a high SNR, while the bulk part of the spectrum can be described with fewer parameters. Therefore, not only the complete infrared difference spectra were fitted, but smaller segments were also individually fitted. By doing this we kept the kinetics of large bands with high SNR from dominating those of small bands with possibly different rate constants.

RESULTS

Not only the pH of a BR sample but also its ionic strength affects the photocycle kinetics (22). Experiments in the visible showed that the amplitudes of the exponentials are very sensitive to the salt and buffer contents while the rate constants remain rather stable between pH 5 and 7 at KCl concentrations between 0 and 4 M. In an amplitude spectrum the amplitude $a_i(\nu)$ of a specific rate constant is plotted as a function of wavenumbers. The M decay turned out to be monophasic at low ionic strength and biphasic at high ionic strength. The ratio of the two decay rate amplitudes depends on pH and ionic strength. In a hydrated film it is more difficult to adjust these parameters to desired values with a reasonable accuracy than in a suspension. In contrast to earlier experiments (17, 18, 24), in this work we used bR samples with high salt and buffer contents, as described in Materials and Methods. The kinetics of the films are identical to those of suspensions at pH 7 in 1 M KCl solution.

Absorbance changes in the visible

In the visible spectral range, absorbance changes were measured at 410, 430, 460, 500, 530, 570, 590, 620, 640, 660, and 680 nm. The global fit analysis gives five rate constants (in agreement with references 2 and 18): k_5 = 70 μs, k_7 = 300 μs, k_4 = 2.3 ms, k_3 = 6.9 ms, and k_6 = 30 ms. Ordering i of the rate constants k_i is according to their significance in the fit calculation (i.e., the fit procedure provides k_3, before k_4). Due to their faster time scale, the K-L transition (k_1 = 1 μs) and the biphasic M rise (k_2 = 30 μs, k_5 = 70 μs) are not resolved. The absorbance band at 410 nm, mainly describing the concentration of the M intermediate, rises with k_5 and decays with k_3, k_4, and k_6 (Fig. 3, *a* and *c*). It should be noted that in contrast to the measurement at 273 K without salt (18), k_4 now contributes significantly to the M decay at 273 and 293 K. The concentration of the O intermediate is largely represented by the absorbance change at 680 nm (Fig. 3, *b* and *d*). Comparing the absorbance changes at 273 and 293 K indicates a significant increase of the apparent O concentration (about four times) at 293 K. The rise of O is dominated by k_4, its decay by k_3. At 293 K, an additional rate, k_7, contributes significantly to O's reaction kinetics.

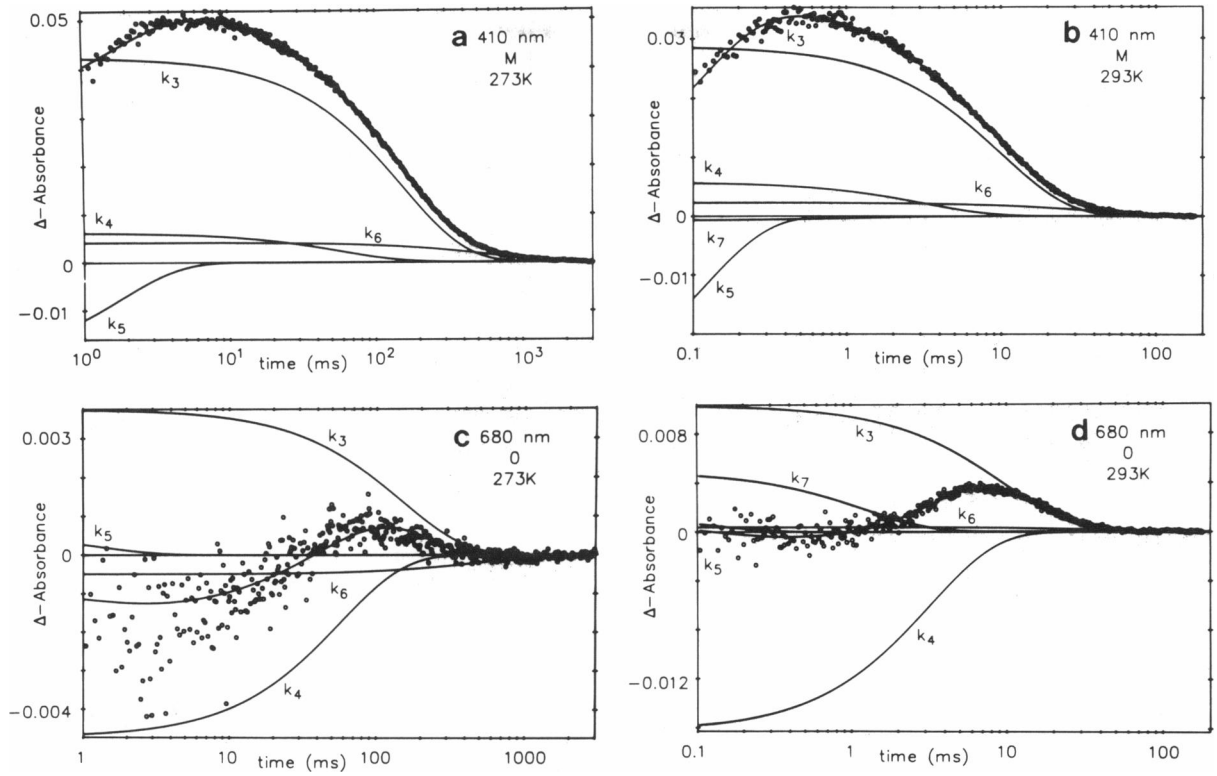

FIGURE 3 Absorbance changes in the visible spectral range. Absorbance changes (*dots*), fitted curve, and the rates k_i by which the fitted curve is composed are shown: (*a*) absorbance change at 410 nm, taken at 273 K; (*b*) absorbance change at 410 nm, taken at 293 K; (*c*) absorbance change at 680 nm, taken at 273 K; (*d*) absorbance change at 680 nm, taken at 293 K.

Amplitude spectra

The amplitude spectra of the apparent rate constants represent mixtures of difference spectra between the BR ground-state and the different intermediates. The contribution of an intermediate to an amplitude spectrum depends on the contribution of the corresponding apparent rate constant to the rise or decay of the intermediate.

Since k_3 describes M decay, N decay, and O decay, the k_3 amplitude spectrum is the sum of $\alpha_3 \cdot$(BR-M) + $\beta_3 \cdot$(BR-N) + $\gamma_3 \cdot$(BR-O) difference spectra (Fig. 4 *a* and *b*). The coefficients α_i, β_i, and γ_i depend on pH, temperature, and ionic strength. As indicated by the small amplitude at 660 nm, the k_3 amplitude spectrum at 273 K represents mainly a mixture of BR-M and BR-N, and at 293 K BR-O also contributes significantly. Due to the overlap of BR and N absorbance bands around 570 nm, the contribution of N is not as clear as those of M (at 410 nm) and of O (at 660 nm). The wavelength dependence of the k_6 amplitude spectrum is similar to the k_3 amplitude spectrum (data not shown). At 293 K its amplitudes are very small but at 273 K they are about half of k_3.

Since k_4 describes M decay, N and O rise to the k_4 amplitude spectra, $\alpha_4 \cdot$(BR-M) − $\beta_4 \cdot$(BR-N) − $\gamma_4 \cdot$(BR-O) difference spectra contribute (Fig. 4 *c* and *d*). N and O contribute to k_4 amplitude spectra with negative amplitudes. Again, O contributes at 293 K much more than at 273 K, as can be seen at 660 nm (Fig. 4, *c* and *d*).

IR-absorbance-changes

In Fig. 5, a three-dimensional graph of the IR absorbance changes at 293 K is shown. In order to smooth the data the fitted curves are presented. In Fig. 6, the difference spectra, measured at 200 μs (*a*) and at 6 ms (*b*) after the laser flash, are shown. The first represents mainly a BR-M difference spectrum with a small L contribution, whereas the second contains N and O contributions.

The fit of the complete IR difference spectra at 293 K clearly requires three time constants: 100 μs, 2.4 ms, and 8.1 ms. The addition of a fourth constant left the two faster unchanged and splits the 8.1-ms rate into two constants of 7.4 and 28.6 ms. The 28.6-ms time constant improves the fit significantly between 1,203 and 1,199 cm^{-1}. Addition of a fifth constant, 300 μs, left the others unchanged and resulted in an improvement between 1,511 and 1,501 cm^{-1}. These five constants seem to be significant not only because of the excellent agreement with those found in the visible (Table 1) but also because of the stability of the fit results. Addition of redundant rates in most cases results in degeneration of rate constants or in a strong dependence on the starting values.

Subsequently, nine smaller segments of the IR spec-

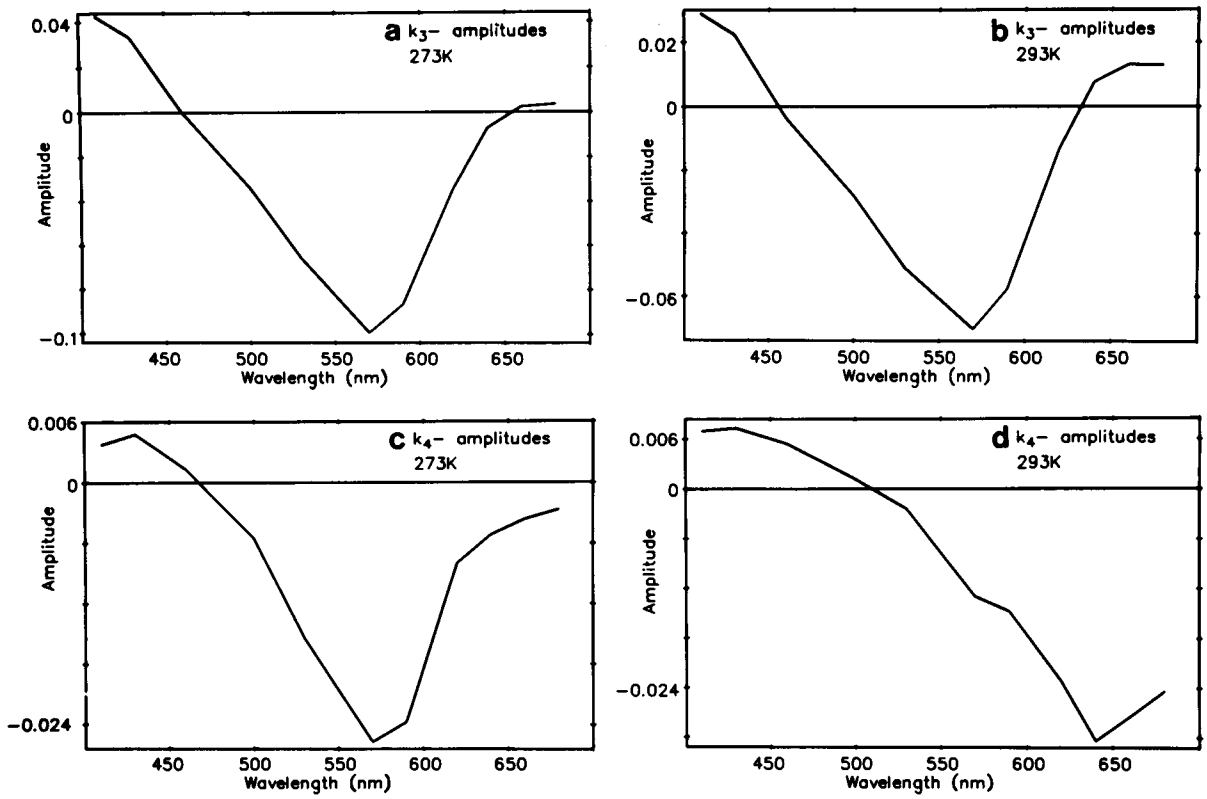

FIGURE 4 Amplitude spectra of the rates k_3 at 273 K (*a*) and 293 K (*b*) and the rate k_4 at 273 K (*c*) and 293 K (*d*).

trum were fitted in order to separate regions dominated by the large chromophore bands from those reflecting mainly smaller protein absorbance changes. The regions selected were 1,790–1,660 cm^{-1} (carbonyl stretching vibrations), 1,691–1,660 cm^{-1}, 1,670–1,650 cm^{-1} (amide-I vibration of the protein backbone), 1,650–1,534 cm^{-1} ($C{=}NH^+$ and ethylenic-stretching vibrations of the chromophore, amide-II vibration of the protein backbone), 1,590–1,480 cm^{-1} (ethylenic-stretching vibrations of the chromophore and amide-II vibration of the protein backbone), 1,580–1,545 cm^{-1} (ethylenic-stretching vibrations of the chromophore and amide-II vibration of the protein backbone), 1,500–1,320 cm^{-1} (protein side groups, chromophore and backbone vibra-

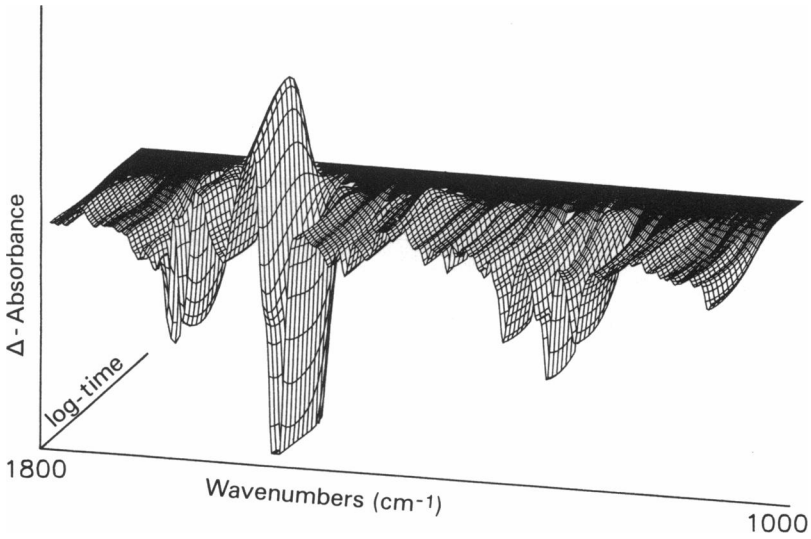

FIGURE 5 Three-dimensional graph of the absorbance changes in the infrared spectral region between 1,800 and 1,000 cm^{-1}. Absorbance bands of the BR groundstate are negative and intermediate bands are positive. The time resolution is 100 μs. In order to smooth the data the fitted curves are shown.

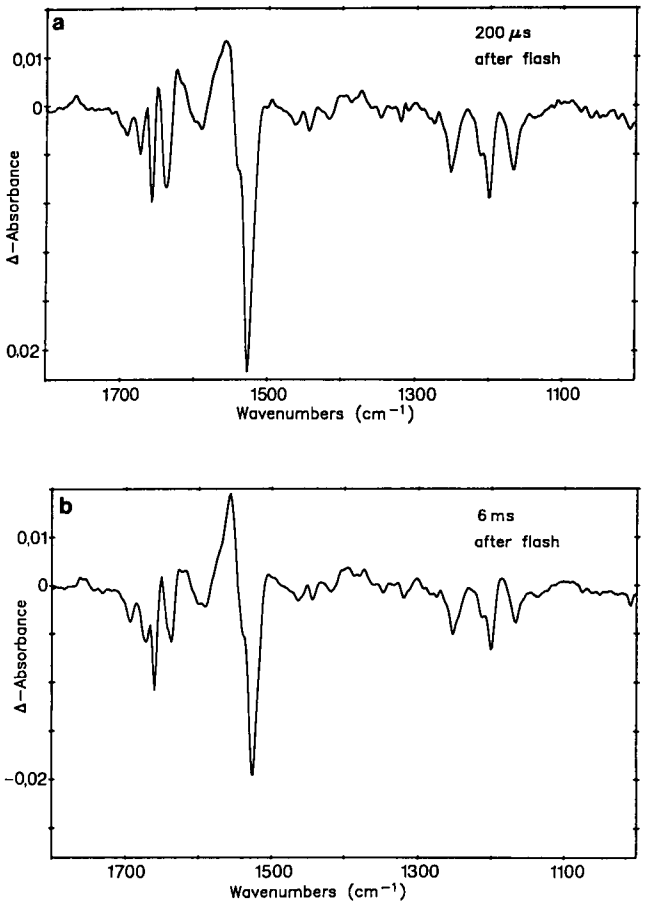

FIGURE 6 Difference spectra taken 200 μs (*a*) and 6 ms (*b*) after the laser flash are shown.

tions), 1,306–1,230 cm^{-1} (protein sidegroups, chromophore and backbone vibrations), 1,230–1,140 cm^{-1} (C—C-stretching vibrations of the chromophore). Depending on S/N, between three and five rate constants were required to fit the data in these segments (see Table 1). The five constants were necessary only between 1,590 and 1,480 cm^{-1} and 1,230 and 1,140 cm^{-1}. In all cases the same rate constants were found as in the visible (410–660 nm). No additional rate constant appeared that could be assigned to a protein reaction which would run asynchronously with the chromophore reactions.

At 1,505 cm^{-1}, representing the ethylenic stretching vibration of the retinal, the O concentration can be followed (Fig. 7 *a* and *b*) (30). Its time dependence agrees with the absorbance change at 660 nm in the visible spectral range. The absorbance change, small at 273 K due to low O concentration, is pronounced at 293 K (Fig. 7 *a* and *b*). Its rise is dominated by k_4 and its decay by k_3. At 293 K, as shown in the visible Fig. 3 *d*, k_7 contributes significantly (Fig. 7 *b*). k_7 indicates O's backreaction to the preceeding intermediates.

The ethylenic stretching vibration of N is seen in resonance Raman experiments at 1,530 and 1,548 cm^{-1} (14, 15). In the infrared difference spectra, in addition, absorbance changes of the amide-II vibration contribute at 1,555 cm^{-1} (18). This may explain the presence of an absorbance band at 1,555 cm^{-1} already in the M intermediate. The further rise of the absorbance changes at 1,555 cm^{-1} is dominated by k_4 decay by k_3 (Fig. 7, *c* and *d*). At 293 K, k_7 also contributes to the rise of this band (Fig. 7 *d*).

Additional absorbance changes representing the concentration of the N intermediate are given in Fig. 8. The absorbance change at 1,186 cm^{-1} represents the reprotonation of the Schiff base after M formation (9, 14, 15, 17, 18, 34). Its rise is dominated by k_4 (Fig. 8 *a* and *b*). At 273 K, at least, it represents mainly the concentration of N, with a minor contribution of O. Measurements at high pH at which the N intermediate accumulates show that the absorbance change at 1,385 cm^{-1} is indicative of N (Gerwert and Souvignier, manuscript in preparation). The rise of this absorbance change is dominated by k_4, decay by k_3 (Fig. 8, *c* and *d*).

In summary, the measurements in the IR indicate that the rise of the N and the O intermediate is dominated by the same rate constant k_4. It seems that k_7 contributes to the decay to preceeding intermediates of O and rise of N.

TABLE 1 Time constants τ_i yielded by global fit analysis in the visible between 410 and 680 nm, in the infrared between 1,800–1,000 cm^{-1} and for different spectral segments; τ_5 = 0.1 ms, τ_2 = 0.3 ms, τ_4 = 2.3 ms, τ_3 = 6.9 ms, τ_6 = 30 ms

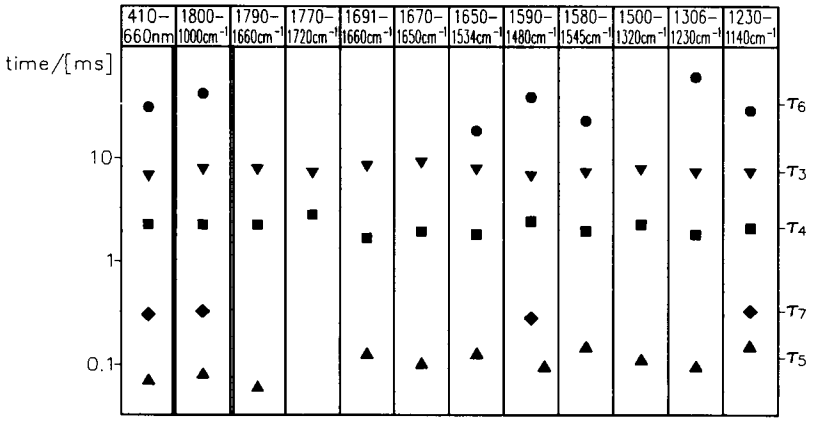

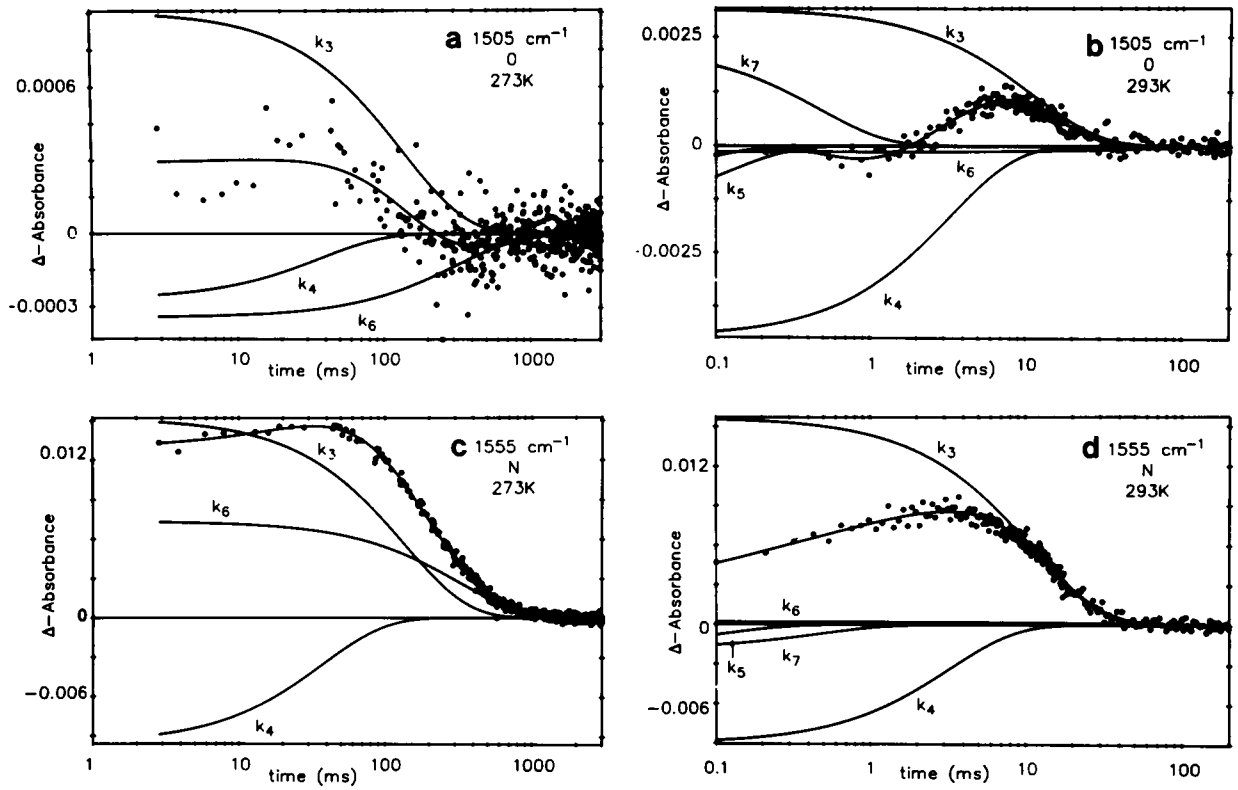

FIGURE 7 Absorbance changes in the infrared spectral region: (*a*) absorbance change at 1,505 cm^{-1} at 273 K; (*b*) absorbance change at 1,505 cm^{-1} at 293 K; (*c*) absorbance change at 1,555 cm^{-1} at 273 K; (*d*) absorbance change at 1,555 cm^{-1} at 293 K.

This can be explained by a fast N ⇄ O equilibrium reaction (3, 26). Alternatively, parallel or branching reactions in M could explain these results.

Amplitude spectra in the IR

The k_3 amplitude spectrum at 273 K (Fig. 9 *a*) represents mostly a BR-M difference spectrum with contributions of BR-N. It resembles the so-called "BR-M" difference spectrum obtained under "steady-state illumination." At 293 K (Fig. 9 *b*), in addition, O contributes, as already shown in the visible's k_3-amplitude spectrum (compare with Fig. 4). The bands characteristic of O are at 1,508 cm^{-1}, a broad band at around 1,170 cm^{-1} and a carbonyl band at 1,732 cm^{-1} (Fig. 9 *b*).

The k_4 amplitude spectrum at 273 K contains almost no O contribution (Fig. 9 *c*), as the corresponding spectrum in the visible indicates. It represents absorbance changes in the BR- to N reaction. It is a superposition of BR-N and BR-M difference spectra α_4 (BR-M) − β_4 (BR-N) in which $\beta \gg \alpha$, i.e., the BR-N difference spectrum dominates. Absorbance bands appearing in N are negative and M bands disappearing in N are positive (compare with Fig. 4 *c*). The characteristics of N are the retinal vibrations at 1,186 cm^{-1}, the band at 1,555 cm^{-1}, the carbonyl vibrations appearing at 1,755 cm^{-1} and disappearing at 1,762 cm^{-1} and disappearing at 1,742 cm^{-1}, the band appearing around 1,396 cm^{-1} and the large amide-I and amide-II difference bands at 1,650 cm^{-1}/ 1,670 cm^{-1} and 1,555 cm^{-1}, respectively. The k_4 amplitude spectrum at 293 K exhibits in addition to these N-specific bands (Fig. 9 *d*), O-specific bands (compare also with Fig. 4 *d*): retinal vibrations around 1,170 cm^{-1} (C—C) and 1,505 cm^{-1} (C=C) (30). The carbonyl vibration at 1,742 cm^{-1} is no longer pronounced and therefore seems to disappear in N but reappear in O. An unidentified carbonyl vibration appears at 1,732 cm^{-1} in O. Interestingly, the 1,755-cm^{-1} asp-carbonyl vibration, more pronounced at 293 K compared with 273 K, indicates protonation of the corresponding asp in O.

DISCUSSION

Photocycle

The global fit analysis proves that four apparent rate constants k_7 = 0.3 ms, k_4 = 2.3 ms, k_3 = 6.9 ms, and k_6 = 30 ms are sufficient to describe the M to BR reaction pathway under physiological conditions. These results agree with earlier findings obtained on hydrated films without salt and buffer (18). The same rate constants describe absorbance changes in the visible and in the different infrared spectral regions, that are indicative of chromophore, side group, and backbone vibrations. This implies a synchronization between reactions in the different molecular groups of the protein not only in the

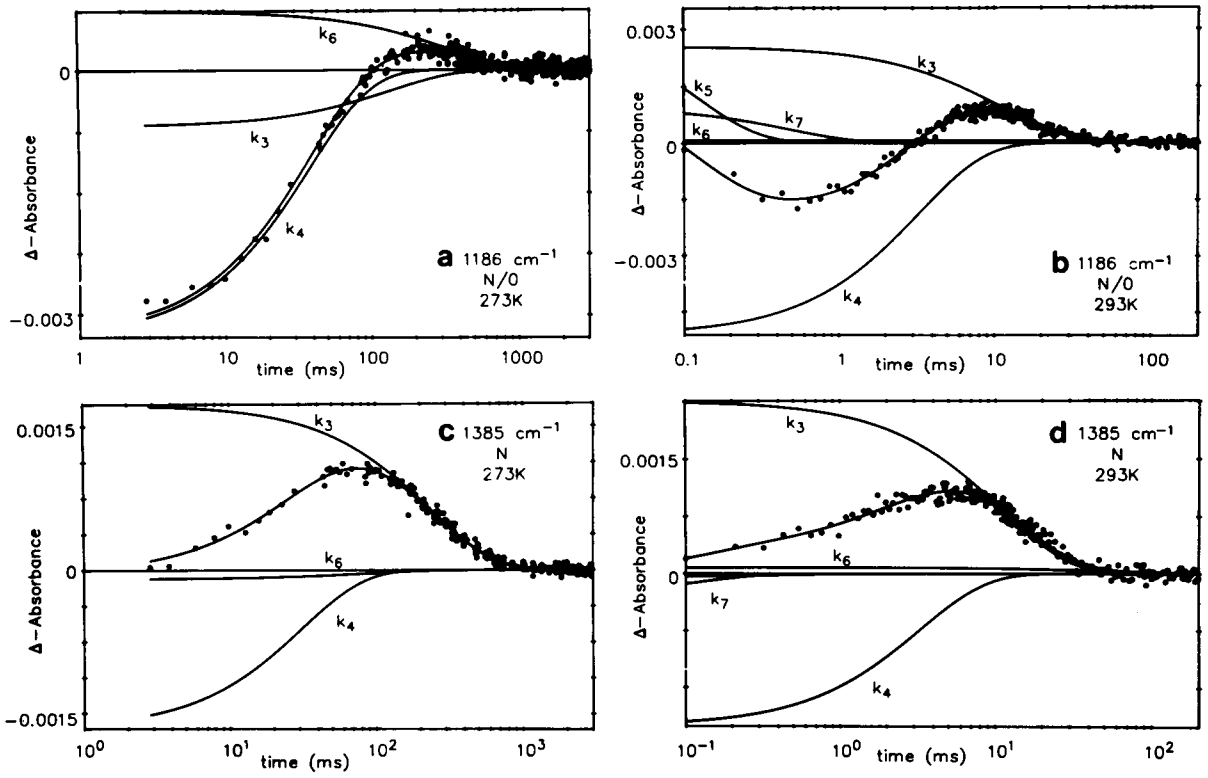

FIGURE 8 Absorbance change in the infrared: (*a*) absorbance change at 1,186 cm^{-1} at 273 K; (*b*) absorbance change at 1,186 cm^{-1} at 293 K; (*c*) absorbance change at 1,385 cm^{-1} at 273 K; (*d*) absorbance change at 1,385 cm^{-1} at 293 K.

ms (18) but also (at least) in the 100-μs time frame under physiological conditions.

In a unidirectional photocycle the apparent rates would correspond to the natural rate constants. For bacteriorhodopsin's photocycle, an unidirectional scheme must be excluded and the apparent rates are functions of several natural rate constants. Therefore, the problem is experimentally underdetermined, i.e., the photocycle model has more parameters than are experimentally accessible. Nevertheless, we will still give the minimal requirements of a photocycle model describing the M to BR reaction pathway. A reasonable model should be able to reproduce the apparent rate constants found in the global fit analysis. Furthermore, the time course of the M concentration should more or less coincide with the absorbance change at 410 nm, that of the O concentration with the absorbance change at 680 nm, and that of N with the absorbance change at 1,385 cm^{-1} (Gerwert and Souvignier, manuscript in preparation). The second of the rates for biphasic M rise is too fast and cannot be experimentally resolved (2). The L to M transition will be discussed elsewhere (Souvignier and Gerwert, manuscript in preparation). The rise of the N and O intermediates should be dominated by k_4. The N and O intermediates should be connected by a fast equilibrium reaction which is reflected by the rate constant k_7. Here we discuss a model with a minimum number of free parameters. It should be noted that more complex models which contain more free parameters are also able to explain our results.

Even the simple scheme:

$$M \rightarrow N \leftrightarrows O \rightarrow BR,$$

can simulate an O concentration which resembles the absorbance change at 680 nm, an M concentration which resembles the absorbance change at 410 nm, and an N concentration which resembles the absorbance change at 1,385 cm^{-1} at low salt concentrations. A possible set of natural time constants k_{xy} which yield the experimentally observed apparent rate constants k_i are given in Table 2. The amplitudes of the apparent rates indicating their contributions to the respective intermediate are given in the table. The data set reveals an interesting point: even if M decays directly to N, its apparent decay is only described by k_3, whereas k_4, which dominates the N and O rise, does not contribute to M's decay. It would have been very difficult to arrive at this conclusion from purely intuitive reasoning. This model scheme clarifies a long discussed ambiguity: because the rise of the 1,755-cm^{-1} asp-carbonyl band is dominated by k_4 but the decay of the 1,762 cm^{-1} asp-carbonyl band is described only by k_3 at low salt concentration, it was concluded that one of two possibilities had to be hold. Either they belong to two different aspartic acids in a linear photocycle (7, 25), or, if not, there must exist parallel photocy-

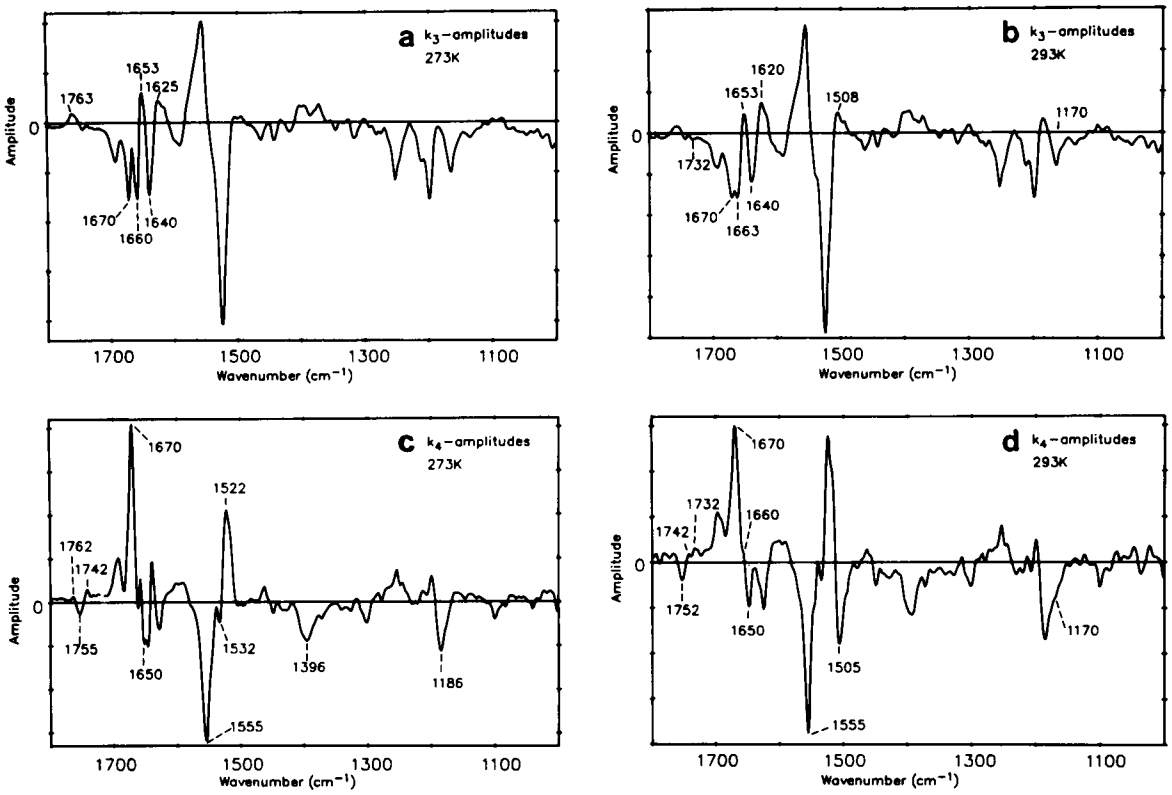

FIGURE 9 Amplitude spectra of k_3 at 273 K (*a*) and 293 K (*b*) and of k_4 at 273 K (*c*) and at 293 K (*d*).

cles (24). The solution outlined here illustrates clearly (in contrast to references 7, 24, 25) that both the 1,762 cm^{-1} and 1,755-cm^{-1} asp-carbonyl vibrations can be assigned to the same aspartic acid in a linear photocycle even if the rate constant describing disappearance of the 1,762-cm^{-1} band, which is connected to M decay, is different from the rate constant describing appearance at 1,755 cm^{-1}, which is connected to N rise.

At high salt concentration the M intermediate and the 1,762-cm^{-1} band decay biphasically with k_3 and k_4, i.e., having a rate constant (k_4) with which the 1,755-cm^{-1} band appears. This supports the conclusion that the asp-85-carbonyl vibration shifts during the M to N transition from 1,762 to 1,755 cm^{-1}. A frequency shift of asp-85 from 1,765 to 1,755 cm^{-1} indicates its environmental change in the M- to N transition.

However, the biphasic M decay cannot be described by the above model. Extending the scheme to the next simpler solution:

$$M \rightleftarrows N \rightleftarrows O \rightarrow BR,$$

can reproduce the biphasic M decay with a large k_3 contribution. One possible set of intrinsic time constants that reproduces the apparent time constants is given in Table 3. The corresponding concentration dependence of M, N, and O is given in Fig. 10. Also, the simultaneous rise of N and O with k_4 and the amplitudes of k_7 are correctly described by this scheme.

The models discussed do not explain the slow rate constant k_6. At physiological conditions its amplitude is very small, and therefore negligible, but at high pH (data not shown) or at low temperature its contribution is of the same order of magnitude as k_4 and k_3. To explain k_6, an additional intermediate in the photocycle has to be introduced. Model simulations with this intermediate situated between O and BR failed to reproduce the experimental data. In this case, the amplitudes calculated for k_6 are too large by at least one order of magnitude. Alternatively, putting the new intermediate in an additional branch, as shown in the following scheme, describes the measured data including k_6 and its amplitudes

$$\begin{array}{l} M \rightleftarrows N \rightleftarrows O \rightarrow BR. \\ \qquad\quad \searrow\ X\ \nearrow \end{array}$$

Alternatively, the rate constant k_6 can be explained by parallel cycles with spectroscopically very similar intermediates and similar intrinsic rate constants for the major part of the reaction (12–14). However, it is not clear if this branching is relevant for the proton-pump mechanism.

In summary, at 20°C, pH 7, and high salt concentration the M to BR reaction can more or less be described by an

$$M \rightleftarrows N \rightleftarrows O \rightarrow BR$$

reaction scheme which agrees with earlier conclusions (3, 15, 26). However, we cannot exclude parallel photo-

TABLE 2 **Natural time constants applying to the photocycle scheme yielding the experimentally observed apparent time constants**

$$M \xrightarrow{k_{MN}} N \underset{k_{ON}}{\overset{k_{NO}}{\rightleftharpoons}} O \xrightarrow{k_{OBR}} BR$$

k_{MN}	k_{NO}	k_{ON}	k_{OBR}
7.1 ms	0.8 ms	0.7 ms	0.7 ms

	k_5	k_7	k_4	k_3
$\tau_{1/2}$ d. k_i	0.07 ms	0.3 ms	2.0 ms	7.1 ms
L	1.0			
M	-1.0			1.0
N	0.01	-0.01	-0.31	0.31
O		0.02	-0.17	0.14

In addition, the amplitudes of the apparent time constants, i.e., their contribution to the respective intermediate kinetic, are given.

TABLE 3 **Natural time constants applying to the photocycle scheme yielding the experimentally observed apparent time constants**

$$M \underset{k_{NM}}{\overset{k_{MN}}{\rightleftharpoons}} N \underset{k_{ON}}{\overset{k_{NO}}{\rightleftharpoons}} O \xrightarrow{k_{OBR}} BR$$

k_{MN}	k_{NM}	k_{NO}	k_{ON}	k_{OBR}
5.0 ms	10.6 ms	1.2 ms	0.7 ms	0.8 ms

	k_5	k_7	k_4	k_3
$\tau_{1/2}$ d. k_i	0.07 ms	0.31 ms	2.2 ms	7.1 ms
L	1.0			
M	-1.0		0.19	0.83
N	0.02	-0.02	-0.52	0.52
O		0.03	-0.20	0.17

In addition, the amplitudes of the apparent time constants, i.e., their contribution to the respective intermediate kinetic, are given.

cycles of different BR groundstate molecules. Nevertheless, under physiological conditions we have presented a sequential scheme with back reactions that can satisfactorily describe the observed multiexponential kinetics. At lower temperature, lower salt concentration, or lower/higher pH, branching or parallel reactions have to be considered to explain k_6.

Because k_4 dominates the rise of N and O, and k_3 dominates their decay, it is reasonable to assume that $\beta_4 \approx \beta_3$ and $\gamma_4 \approx \gamma_3$. In this case the addition of the amplitude spectra $k_4 + k_3$ with k_4 ($=\alpha_4$ (BR-M) $- \beta_4$ (BR-N) $- \gamma_4$ (BR-O)) and k_3 ($=\alpha_3$ (BR-M) $+ \beta_3$ (BR-N) $+ \gamma_3$ (BR-O)) represents a pure BR-M-difference spectrum (Fig. 11 *a*, visible; Fig. 11 *b*, infrared). Comparison with Fig. 9 *d* shows that the so-called "BR-M" difference spectrum obtained under steady-state illumination represents mainly BR-M with a minor contribution of the BR-N difference spectra (9). Deviations to the low temperature BR-M difference spectrum (Fig. 11 *c*) are caused by N contributions, but do not verify, as recently proposed, a second M intermediate (23). Interestingly, a comparison of the low temperature BR-M with the "pure" room temperature BR-M difference spectrum shows mainly deviations in the amide-I (1,650/1,660 cm^{-1}) and amide-II regions (1,550 cm^{-1}). The conformational change of the backbone is frozen at the low temperature (compare Fig. 11, *b* and *c*). This seems to prevent the reprotonation of the Schiff base, stops the photocycle in M, and thereby shuts off proton pump activity. These conclusions agree with references 23, 31.

In order to yield vectoriality, conceptionally, two different intermediates have to exist: (*a*) one with access of the C=NH$^+$ to the proton release pathway; and (*b*) one with access of the C=N to the proton uptake pathway.

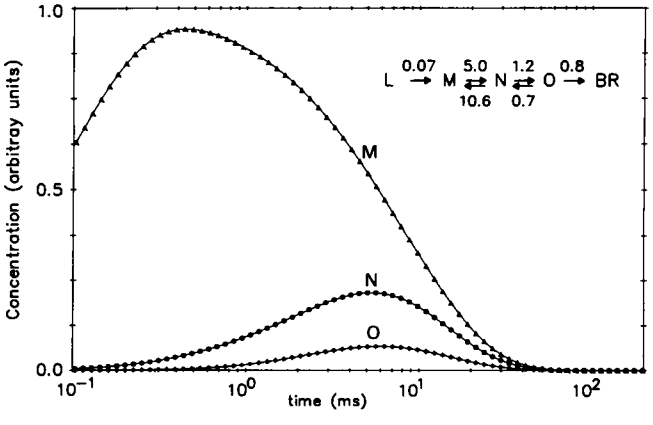

FIGURE 10 Calculated concentration dependence of the M, N, and O intermediates of the model scheme using the given natural time constants.

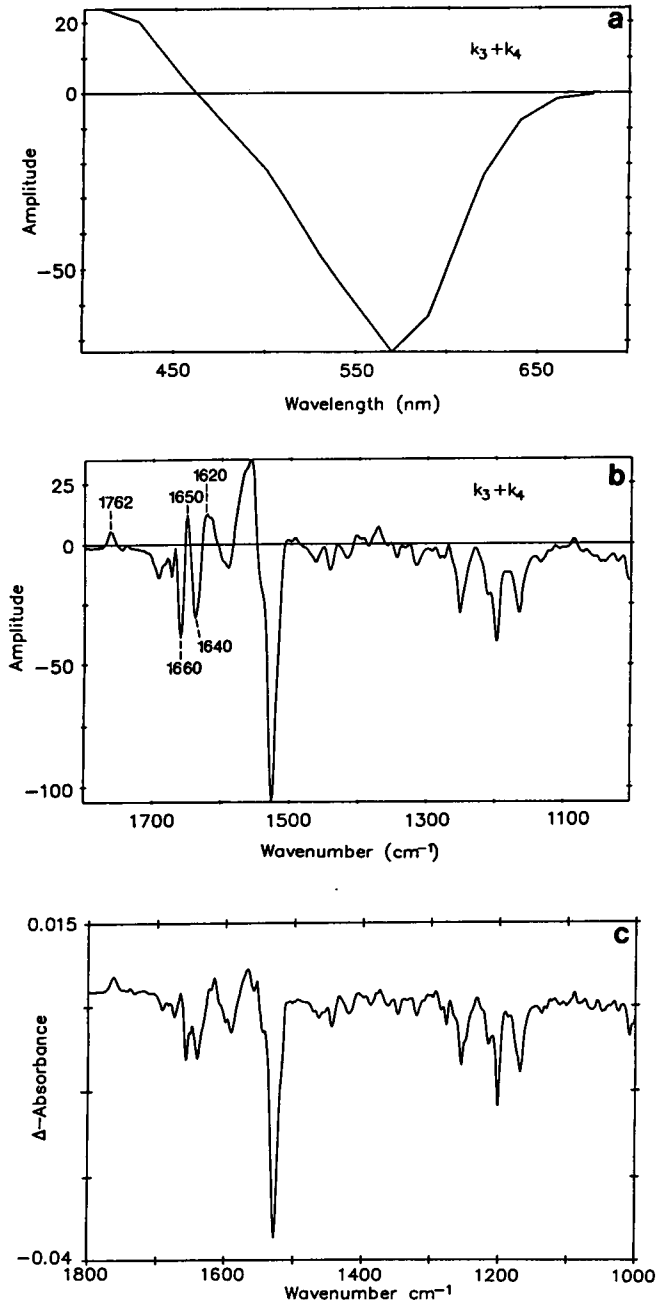

FIGURE 11 $k_3 + k_4$ amplitude spectra yielding a "pure" BR-M difference spectra in the visible (*a*) and infrared (*b*). In addition, a low temperature BR-M difference spectrum is shown (*c*).

This proton pump's reset switch was assigned either to the C_{14}—C_{15} single bond isomerization (32) or to a pure protein conformational change (33). Mechanistically, it was signified as an M_1 to M_2 transition (3, 7, 32) or attributed to the L to M transition (33). Our results do not indicate the existence of two different M intermediates at room temperature, and model simulation of the data do not suggest such possibilities. The low temperature BR-M difference spectrum, which differs from the room temperature BR-M only in its protein configuration, could represent an M_1 but is experimentally not observed at room temperature. Nevertheless, conceptionally, there have to exist two M states, one with orientation of the Schiff base to the proton acceptor asp 85 and one with orientation of the Schiff base to the proton donor asp 96. A very fast reprotonation of the Schiff base may merge the M_2 and N intermediates making their experimental detection impossible.

Proton pump model

In the following, we attribute reactions to different intermediates to obtain a dynamic picture of the pump. Even if the N and O intermediates are connected via a fast equilibrium reaction we can still distinguish between reactions with N and as reactions from those with O, by comparing k_4-amplitude spectra at 273 and at 293 K (Fig. 9, *c* and *d*). The results in the visible and in the infrared indicate almost no apparent O contribution during the M to BR reaction at 273 K and a significant O contribution at 293 K.

The following conclusions can be drawn (and are illustrated in Fig. 12): (*a*) because the 1,742-cm^{-1} band, indicative of asp-96 deprotonation (9, 18), clearly disappears in N but not in O, asp-96 deprotonates during the M to N transition and reprotonates already in the N to O transition; (*b*) the carbonyl vibration of asp-85 seems to shift from 1,761 cm^{-1} in the M intermediate to 1,755 cm^{-1} in the N and O intermediate; this indicates an environmental change of asp-85 during the M to N (conceptionally M_2) transition which persists in O. This conclusion is in agreement with a recent assignment of the 1,755 cm^{-1} carbonyl band to asp-85 (F. Siebert, private communication). Its protonation explains the red-shift in the O intermediate, because the asp-85's counterion does not stabilize the positive chromophore charge; (*c*) the amide-I and II difference bands at 1,670/1,650 cm^{-1} and at 1,555 cm^{-1}, indicative of a conformational change of the protein backbone, are the largest in N. This conformational change in the M to N transition is blocked at low temperature, at which the proton uptake is inhibited; therefore, we conclude that this conformational change is essential for the proton uptake mechanism. It takes place in the M to N (conceptionally in the M_2) transition, but not in the L to M as proposed by the C-T model (33). In time-resolved x-ray diffraction studies structural alterations of a few amino acid residues at both ends of the retinal at helix G and between the helices E and F are observed, which might be caused by a tilt of α-helices (27). The structural relaxation is related to the M's decay but occurs after the first phase. This result is in full agreement with the absorbance changes of the amide-I and II vibration observed here. In agreement with the diffraction studies large scale structural changes during bacteriorhodopsin's photocycle can be excluded; the IR-absorbance changes indicate involvement of only one to three residues. The time course of the structural change, clearly elucidated in the IR experiments, proves

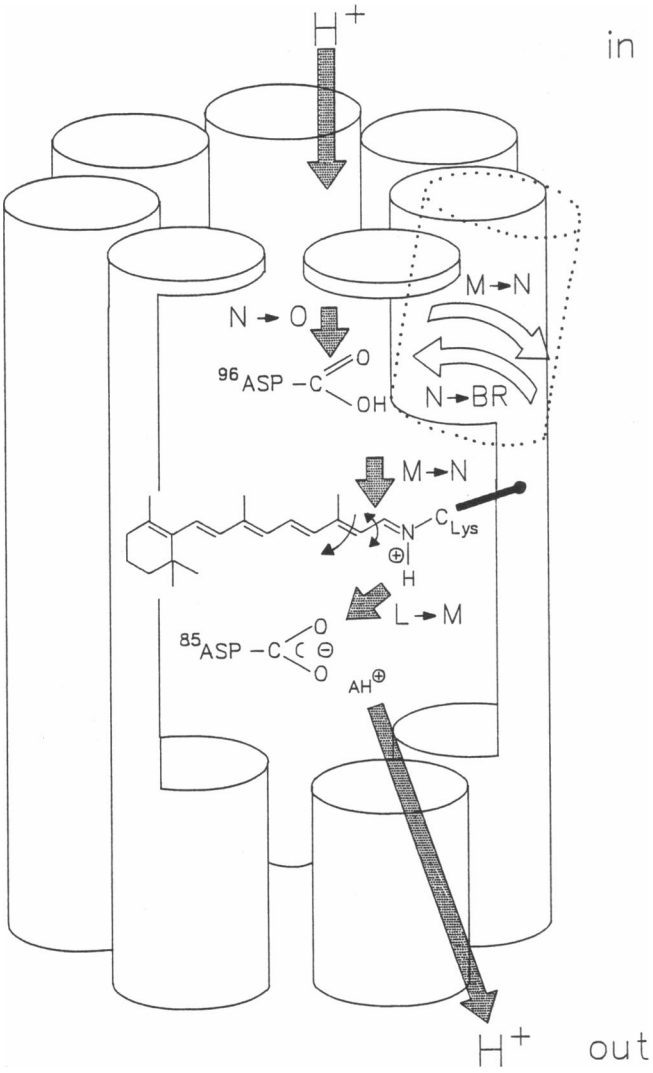

FIGURE 12 Model of the proton-pump mechanism. After light induced $C_{13}=C_{14}$ double band isomerization and twist around the $C_{14}-C_{15}$ single bond, the pK of the protonated Schiff base is reduced. In the L to M transition a proton is transfered from $C=NH^+$ to asp 85. Because a proton is released in the L to M transition another proton donor group has to be involved in the proton-release mechanism (AH^+). After relaxation around the light induced twist of the $C_{14}-C_{15}$ single bond and a structural change, maybe of helix G, in the M to N transition, the Schiff base can be reprotonated in the M to N transition from asp 96. Bound water molecules may be involved in the reprotonation pathway. Asp 96 is already reprotonated in the N to O transition.

that it is largest in the M to N (conceptionally M_2) transition and relaxes during the N to BR reaction. We conclude that the absorbance changes of the amide I and II vibrations are most likely caused by a structural backbone change close to helix G and helices F and E; (*d*) the broad continuum band above 1,765 cm^{-1} disappears in the M to N reaction. This may indicate a change in a hydrogen-bonded network, which could transport protons in an ice-like mechanism (18, 28); (*e*) the carbonyl vibration of an additional unidentified protonated carboxylic acid at 1,732 cm^{-1} appears in O.

A further development of the stroboscopic-FTIR technique should yield a time resolution of 25 μs in the near future. This will allow us to examine the L to M reaction.

We thank Regina Eichas-Nell for her excellent technical help, Benedikt Heßling and Johannes le Coutre for their help with the measurements, and Dr. David Rumschitzki for reading the manuscript. We thank K. H. Müller and Dr. Th. Plesser for providing the global-fit program.

A Heisenberg-fellowship to K. Gerwert of the Deutsche Forschungsgemeinschaft and grant Ge 599/7-1 are gratefully acknowledged.

Received for publication 26 February 1992 and in final form 9 June 1992.

REFERENCES

1. Tittor, J. 1991. A new view of an old pump: bacteriorhodopsin. *Current Opinion in Structural Biology.* 1:534–538.
2. Xie, A. H., J. F. Nagle, and R. H. Lozier. 1987. Flash spectroscopy of purple membrane. *Biophys. J.* 51:627–635.
3. Váró, G., and L. Lanyi. 1990. Pathways of the rise and decay of the M photointermediate(s) of bacteriorhodopsin. *Biochemistry.* 29:2241–2250.
4. Lugtenburg, J., R. A. Mathies, R. G. Griffin, and J. Herzfeld. 1988. Structure and function of rhodopsins from solid state NMR and resonance Raman spectroscopy of isotopic retinal derivatives. *TIBS.* 13:388–393.
5. Kitagawa, T., and A. Maeda. 1989. Vibrational spectra of rhodopsin and bacteriorhodopsin. *Photochem. Photobiol.* 50:883–894.
6. Braiman, M. S., and K. J. Rothschild. 1988. Fourier transform infrared techniques for probing membrane protein structure. *Ann. Rev. Biophys. Biophys. Chem.* 17:541–570.
7. Engelhard, M., K. Gerwert, B. Hess, W. Kreutz, and F. Siebert. 1985. Light-driven protonation changes of internal aspartic acids of bacteriorhodopsin: an investigation by static and time-resolved infrared difference-spectroscopy using [4-^{13}C]aspartic labeled purple membrane. *Biochemistry.* 24:400–407.
8. Gerwert, K., and F. Siebert. 1986. Evidence for light-induced 13-cis, 14-s-cis isomerization in bacteriorhodopsin obtained by FTIR difference-spectroscopy using isotopically labelled retinals. *EMBO J.* 5:805–811.
9. Gerwert, K., B. Hess, J. Soppa, and D. Oesterhelt. 1989. Role of aspartate-96 in proton translocation by bacteriorhodopsin. *Proc. Natl. Acad. Sci. USA.* 86:4943–4947.
10. Trissl, H. W. 1990. Photoelectric measurements of purple membranes. *Photochem. Photobiol.* 51:793–818.
11. Lozier, R. H., R. A. Bogomolni, and W. Stoeckenius. 1975. Bacteriorhodopsin: a light-driven proton pump in Halobacterium halobium. *Biophys. J.* 15:955–962.
12. Hanamoto, J. H., P. Dupuis, and M. A. El-Sayed. 1984. On the protein (tyrosine)-chromophore (protonated Schiff base) coupling in bacteriorhodopsin). *Proc. Natl. Acad. Sci. USA.* 81:7083–7087.
13. Dancsházy, Zs., R. Govindjee, and T. G. Ebrey. 1988. Independent photocycles of the spectrally distinct forms of bacteriorhodopsin. *Proc. Natl. Acad. Sci. USA.* 85:6358–6361.
14. Diller, R., and M. Stockburger. 1988. Kinetic resonance Raman studies reveal different conformational states of bacteriorhodopsin. *Biochemistry.* 27:7641–7651.
15. Fodor, S. P. A., J. B. Ames, R. Gebhard, E. M. M. van den Berg, W. Stoeckenius, J. Lugtenburg, and R. A. Mathies. 1988. Chromophore structure in bacteriorhodopsin's N intermediate: im-

plications for the proton-pumping mechanism. *Biochemistry.* 27:7097–7101.

16. Souvignier, G., and K. Gerwert. 1991. Time-resolved FTIR studies on proteins. SPIE, Proceedings of the 8th International Conference on Fourier-Transform-Spectroscopy. 1575:431–432.
17. Braiman, M. S., O. Bousché, and K. J. Rothschild. 1991. Protein dynamics in the bacteriorhodopsin photocycle: submillisecond Fourier transform infrared spectra of the L, M, and N photointermediates. *Proc. Natl. Acad. Sci. USA.* 88:2388–2392.
18. Gerwert, K., G. Souvignier, and B. Hess. 1990. Simultaneous monitoring of light-induced changes in protein side-group protonation, chromophore isomerization, and backbone motion of bacteriorhodopsin by time-resolved Fourier-transform infrared spectroscopy. *Proc. Natl. Acad. Sci. USA.* 87:9774–9778.
19. Gerwert, K. 1988. Intramolekulare Proteindynamik untersucht mit zeitaufgelöster Fourier Transform Infrarot-Differenzspektroskopie. *Ber. Bunsenges. Phys. Chem.* 92:978–982.
20. Oesterhelt, D., and W. Stoeckenius. 1974. *Methods Enzymol.* 31:667–678.
21. Mantz, A. W. 1976. *Appl. Spectrosc.* 30:459.
22. Kouyama, T., A. Nasuda-Kouyama, A. Ikegami, M. K. Mathew, and W. Stoeckenius. 1988. Bacteriorhodopsin photoreaction: identification of a long-lived intermediate N/P R350 at high pH and its M-like photoproduct. *Biochemistry.* 27:5855–5863.
23. Ormos, P. 1991. Infrared spectroscopic demonstration of a conformational change in bacteriorhodopsin involved in proton pumping. *Proc. Natl. Acad. Sci. USA.* 88:473–477.
24. Müller, K.-H., H. J. Butt, E. Bamberg, K. Fendler, B. Hess, F. Siebert, and M. Engelhard. 1991. The reaction cycle of bacteriorhodopsin: An analysis using visible absorption, photocurrent and infrared techniques. *Eur. Biophys. J.* 19:241–251.
25. Siebert, F., W. Maentele, and W. Kreutz. 1982. Evidence for the protonation of two internal carboxylic groups during the photocycle of bacteriorhodopsin. *FEBS Lett.* 141:82–87.
26. Chernavskii, D. S., I. V. Chizhov, R. H. Lozier, T. M. Murina, A. M. Prokhorov, and B. V. Zubov. 1989. Kinetic model of bacteriorhodopsin photocycle: pathway from M state to bR. *Photochem. Photobiol.* 49:649–653.
27. Koch, M. H. J., N. A. Dencher, D. Oesterhelt, H.-J. Plöhn, G. R. Rapp, and G. Büldt. 1991. Time-resolved x-ray diffraction study of structural changes associated with the photocycle of bacteriorhodopsin. *EMBO J.* 10:521–526.
28. Zundel, G. 1988. Proton transfer in and proton polarizability of hydrogen bonds: IR and theoretical studies regarding mechanisms in biological systems. *J. Mol. Struc.* 177:43–68.
29. Bousche, O. M. Braiman, Yi-Wu He, T. Marti, H. Gobind Khorana, and K. J. Rothschild. 1991. Vibrational spectroscopy of bacteriorhodopsin mutants. *J. Biol. Chem.* 266:11063–11067.
30. Smith, S. O., J. A. Pardoen, P. P. J. Mulder, B. Curry, J. Lugtenburg, and R. Mathies. 1983. Chromophore structure in bacteriorhodopsin's O_{640} photointermediate. *Biochemistry.* 22:6141–6148.
31. Gerwert, K., R. Rodriguez-Gonzales, and F. Siebert. 1985. Time-resolved infrared spectroscopy applied to photobiological systems. Time-Resolved Vibrational Spectroscopy. Springer-Verlag, Berlin. 259–262.
32. Schulten, K., and P. Tavan. 1979. *Nature (Lond.).* 272:85.
33. Ames, J. B., and R. A. Mathies. 1990. The role of back-reactions and proton uptake during the N → O transition in Bacteriorhodopsin's photocycle: a kinetic resonance Raman study. *Biochemistry.* 29:7181–7190.
34. Pfefferlé, J. M., A. Maeda, J. Sasaki, and T. Yoshizawa. 1991. Fourier transform infrared study of the N intermediate of bacteriorhodopsin. *Biochemistry.* 30:6548–6556.
35. Müller, K. H., and Th. Plesser. 1991. Variance reduction by simultaneous multi-exponential analysis of data sets from different experiments. *Eur. Biophys. J.* 19:231–240.